Machining Science and Technology
An International Journal

ISSN: 1091-0344 (Print) 1532-2483 (Online) Journal homepage: http://www.tandfonline.com/loi/lmst20

Influence of tool inclination on chip formation process and roughness response in ball-end milling of freeform surfaces on Ti-6Al-4V alloy

Jorge Andrés García-Barbosa, José Manuel Arroyo-Osorio & Ernesto Córdoba-Nieto

MACHINING SCIENCE AND TECHNOLOGY
2017, VOL. 21, NO. 1, 121–135
http://dx.doi.org/10.1080/10910344.2016.1260434

Influence of tool inclination on chip formation process and roughness response in ball-end milling of freeform surfaces on Ti-6Al-4V alloy

Jorge Andrés García-Barbosa [a], José Manuel Arroyo-Osorio [b], and Ernesto Córdoba-Nieto [b]

[a]Facultad de Ingeniería Mecánica, Universidad Santo Tomás (Colombia), Bogotá, Colombia; [b]Departamento de Ingeniería Mecánica y Mecatrónica, Universidad Nacional de Colombia, Bogotá, Colombia

ABSTRACT

An experimental test part, which was made up of flat, concave, and convex surfaces of variable curvatures, was designed to be fabricated in a four-axis machining center. Aluminum alloy 7075 and titanium alloy *Ti-6Al-4V* were used for the fabrication. Within the finishing process, smeared/adhered material was found in some areas of the concave and convex surfaces of the titanium alloy. On the other hand, smeared/adhered material was not found in the aluminum alloy. To characterize the type of defects, the 3D roughness parameters of the surfaces were measured by confocal microscopy, and surface morphology was observed using optical microscopy and scanning electron microscopy. The kinematics of the ball-end milling process was modeled and it was found that the lead and tilt angles between the tool axis and surface normal vector vary continuously, producing transitions between oblique-plunge-push-up milling and oblique-reverse-push-up milling. This causes variation in the thickness behavior during the chip formation process. It was found that the lead angle has a moderate influence, while the tilt angle has a strong effect on the quality of the surfaces of the titanium alloy, with negative tilt angles producing the worst surfaces when there was the oblique-plunge-push-up milling process.

KEYWORDS

Ball-end milling; freeform surfaces; multiaxis machining; surface quality; tool orientation

Introduction

Titanium alloys are used for the fabrication of a great variety of components in the aerospace, chemical, and medical industries due to its excellent relation between mechanical resistance and weight (Ezugwu and Wang, 1997), corrosion resistance and good performance at high temperatures (Sun and Guo, 2009). The machining process is used in the production of titanium alloy parts. However, these alloys are classified within the category of difficult-to-cut materials (Cheharon and

CONTACT Jorge Andrés García-Barbosa jorgegarcia@usantotomas.edu.co Facultad de Ingeniería Mecánica, Universidad Santo Tomás (Colombia), Carrera 9 No. 51-11, Bogotá, Colombia.

Jawaid, 2005) due to their low thermal conductivity, high chemical reactivity, relatively low modulus of elasticity (Guo et al., 2009), and their peculiar work-hardening characteristics (Donachie, 2000). The CNC multiaxis machining process with a ball-end tool is commonly used to obtain freeform surfaces, which are formed by zero, positive, and negative curvature surfaces (Lin and Koren, 1996). In these conditions, variables like the material of the part, the tool inclination angle with respect to the surface normal vector, the change of the transversal section of the chip, and the variation of the stress and strain tensors, have a direct influence on tool vibration (Quinsat et al., 2011), which produces anisotropic changes in the superficial roughness (Becze et al., 2000). The quality of the surface is critical for the performance of components in mechanical, electronic, and biomedical systems. Therefore, most of the fabricated parts with titanium alloys include machining in their production process, particularly the milling process with ball-end milling tools (Ezugwu and Wang, 1997).

Several studies have been published about surface defects produced by milling machining on titanium alloys. Thomas et al. (2010) reported plastic deformation in the form of intense slip bands in slab milling of *Ti-6Al-4V* and Ti-834. Ginting et al. (2009) conducted toroidal end milling experiments on Ti-6242S high-temperature titanium alloy. The defects reported were lay pattern and feed marks, a natural defect because of effective cutting movement; tearing surface, probably produced by built-up edge and attrition removal of work material; microchip or debris deposited on the machined surface at high cutting condition; built-up layer or BUL, as it has been denominated by the above-mentioned authors, which is a chip layer formation caused by molten chip deposited on the machined surface. As noted by these authors, further study is needed to understand the formation of the BUL. Mhamdi et al. (2012) performed ball-end milling experiments in three-axis milling of *Ti-6Al-4V* with finishing cutting conditions to generate a concave surface with a single curvature. Said authors found a surface topography with heavy plastic deformations, which are characterized by ridges caused by the kinematics of the process. Li et al. (2011) did face-down milling tests on *Ti-6Al-4V* alloy. At lower cutting speed, the machined surface was relatively smooth, while at higher cutting speed, the 3D surface topography of the machined surface showed a large number of aspirate peaks. The temperature of the cutting zone increases as a consequence of the higher cutting speed. Thus, the temperature had a significant and adverse effect on the surface quality. Hood et al. (2014) conducted ball-end milling experiments on burn-resistant titanium alloy. They machined flat surfaces with an inclination angle of 0° and 45° in the feed direction. Workpiece surface/subsurface damage was observed in all of the tests. This included carbide pullout or fracture, smeared/adhered material, and microcracks. The severity of these features depended on the operating parameters used with higher levels, generally yielding more damage.

In the present work, a finishing milling process was performed with a ball-end tool to obtain freeform surfaces on titanium *Ti-6Al-4V* and aluminum 7075 alloys. The objective was to understand the cause of the smeared/adhered material formation, which occurs in the machining of the titanium alloy by means of

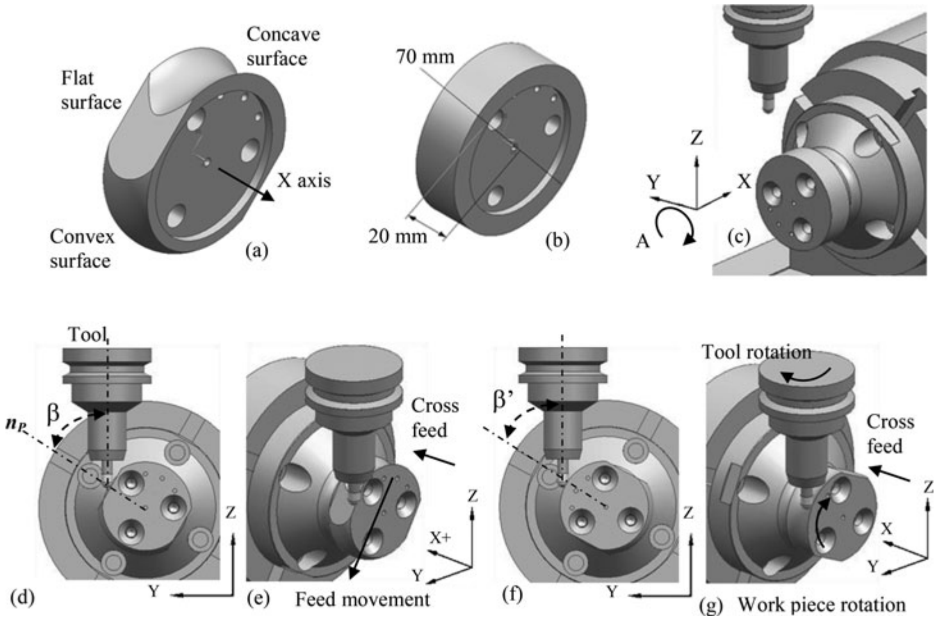

Figure 1. Test workpiece (a). Dimensions of raw material (b). Setup on fourth axis machine (c). Setup for the finishing process for the flat surfaces (d, e) and concave surface (f, g).

modeling of the kinematics behavior of the milling process and the process of chip formation.

Materials and methods

Work material and workpiece setup

Figure 1a shows the part designed for the test. It is made up of flat, concave, and convex surfaces of variable curvature, to study the process of the multiaxis milling with a ball-end tool. A raw material with 70 mm diameter and 20 mm thickness was chosen. A vertical machining center with a rotational fourth axis was chosen for the manufacturing process. The assembly is shown in Figure 1c. The flat surfaces are parallel to the cylinder revolution axis that represents the raw material. The concave and convex surfaces were generated through the partial revolution of an elliptical section around the *X*-axis. The working materials used were *Ti-6Al-4V* ELI (Grade 23) titanium alloy with a composition in weight percent of 6.05 Al, 3.93 V, 0.08 C, 0.006 N, 0.019 H, 0.13 Fe, 0.12 O, and Ti completing the balance; and the 7075 aluminum alloy with a composition in weight percent of 0.4 Si, 0.5 Fe, 1.3 Cu, 0.3 Mn, 2.4 Mg, 0.25 Cr, 5.5 Zn, 0.2 Ti, and Al completing the balance. Table 1 shows the main mechanical properties of these alloys.

Milling strategy

For all surfaces, a roughing process leaving 0.25 mm of stock allowance for the finishing process was performed. For the finishing processes on the flat surfaces,

Table 1. Mechanical properties of aluminum alloy 7075 and titanium alloy *Ti-6Al-4V* ELI.

Material	Ultimate tensile strength (MPa)	Modulus of elasticity (GPa)	Density (g/cm^3)	Thermal conductivity (W/m·K)	Elongation at break (%)	Hardness (HV)
Ti-6Al-4V ELI	860	113	4.43	6.7	15	341
Aluminum alloy 7075	572	72	2.81	130	11	175

inclination lead angles $\beta = -25°$ and $-60°$, in the feed direction, between the tool axis and the surface normal vector $\boldsymbol{n}_{\mathbf{P}}$ were considered, as shown in Figure 1d. The feed movement was done from top to bottom, applying the push-up milling strategy, according to the nomenclature proposed by Bouzakis et al. (2003) (Figure 1e), with increments in the cross-feed direction ($X+$). Considering the 0.25 mm of stock allowance, the inclination lead angles β were selected to avoid the plowing phenomenon (there is no chip formation, but there is elastic and plastic deformation) (Fagali de Souza et al., 2014).

For the finishing process on the concave and convex surfaces, a constant lead angle between the tool axis and surface normal vector projection on the Y–Z plane ($\beta = -25°$ and $-60°$) (Figure 1f) was selected. The feed movement was obtained by rotating the fourth axis in the direction shown in Figure 1g. The machining process was performed in dry conditions and the cutting parameters recommended by the ball-end mill manufacturer for titanium alloys were used 60 m/min cutting speed, 0.03 mm feed per tooth, 0.50 mm cross-feed, and 0.25 mm axial depth of cut.

Machine tool, cutting tool setup, and characterization equipment

The machine tool used was a Leadwell V-20 vertical machining center with 8,000/min^{-1} maximum spindle speed and 5.5 kW power. This machine has the stiffness, accuracy, and repeatability characteristics of a general-purpose machining center, in agreement with the test certificate supplied by the manufacturer. An estimate of our technological setup (Figure 1) stiffness gives a value of 7.2 N/μm (García-Barbosa et al., 2014). The machine was equipped with a fourth rotational axis Golden Sun CNC-151R with 22/min^{-1} maximum rotational speed, 225N maximum torque, and 0.001° positioning precision. The Fanuc 0MD controls the four available axes. In the finishing machining process, an 8 mm diameter ball-end mill (reference Kennametal® F3AW0800AWL35E160) was used. It has a 35° edge angle, 3 cutting edges, and KCPM15-grade material, coated carbide with a coating deposited by physical vapor deposition (PVD). The cantilever of the tool was 20 mm in a Kennametal® hydraulic tool holder. A run-out of 0.011 and 8.015 mm effective diameter were measured in the ball-end mill using a Zoller-Smile-400 tool presetting machine. After the finishing process, the surface microtopography was observed using an FEI® Quanta 200 model scanning electron micoscope (SEM).

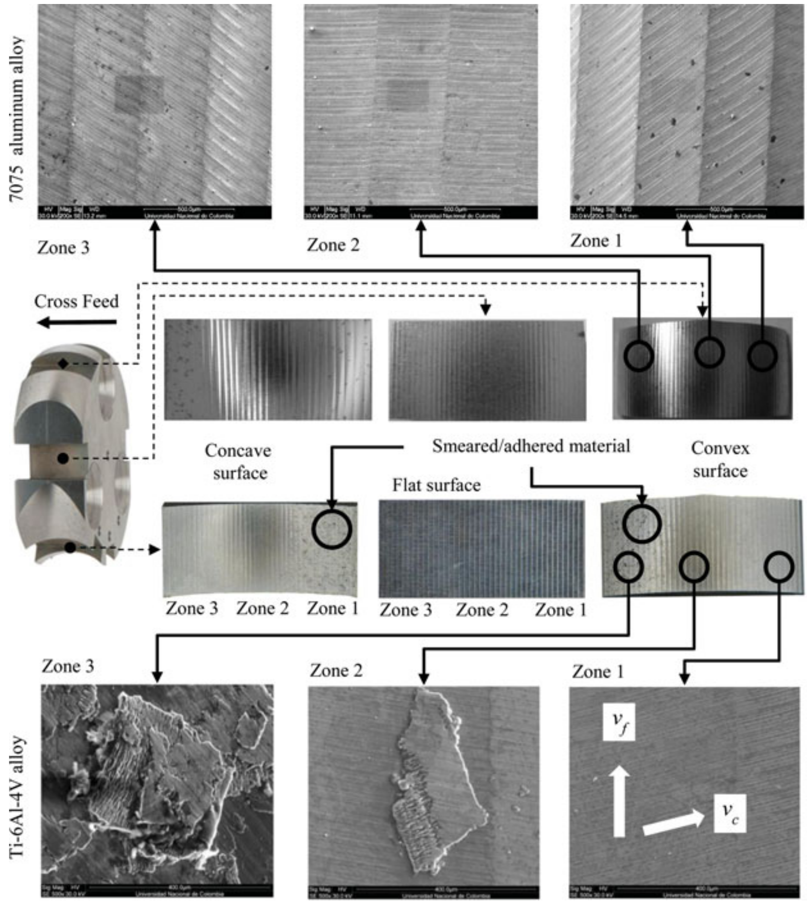

Figure 2. Samples of the machined surfaces ($\beta = -25°$). Scanning electron microscope images of three areas of the concave surface of 7075 alloy (200×) and *Ti-6Al-4V* alloy (500×).

The surface roughness was evaluated with a Carl Zeiss® LSM700 confocal microscope.

Experimental results

Figure 2 shows images of the machined surfaces with a $\beta = -25°$ lead angle. A homogeneous roughness is observed in the 7075 aluminum alloy on the flat, concave, and convex surfaces, whereas the roughness observed on the flat surface in the *Ti-6Al-4V* alloy is homogeneous, a nonhomogenous roughness is seen on the concave and convex surfaces. They present a variation in roughness, from a similar state to that observed on the flat surface, to a bad surface quality. This variation is characterized by smeared/adhered material, as was reported by Hood et al. (2014). This defect appears intensively on the concave surface (Zone 1) at the beginning of the finishing process, while the defect is seen in the final passes of the finishing process on the convex surface (Zone 3).

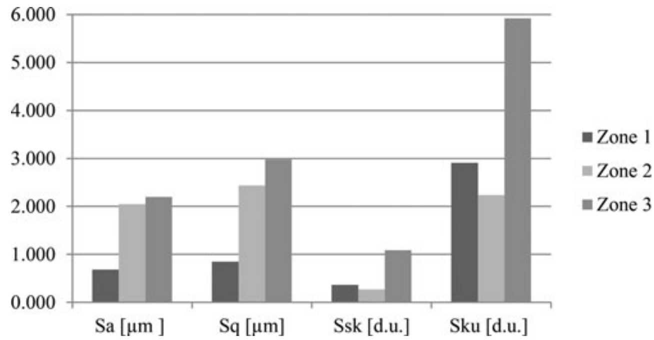

Figure 3. Roughness parameters in Zones 1, 2, and 3 of the convex surface ($\beta = -25°$) of *Ti-6Al-4V* alloy.

The SEM images of the *Ti-6Al-4V* alloy convex surface (Figure 2) show feed marks in Zone 1; a single smeared partially formed chip in Zone 2; and many partially formed chips, smeared and overlapped in Zone 3. Some microchip or debris was also observed, but other defects reported by Ginting et al. (2009), such as lay pattern, tearing surface, or molten chip deposited on the machined surface, were not observed. Smeared and adhered material also appeared, but with a lower intensity, on the concave and convex surfaces machined with a $\beta = -60°$ lead angle.

Figure 3 shows the roughness values on the convex surface. They were obtained with confocal microscopy and according to the ISO 25178 norm. It can be observed that S_a and S_q amplitude parameters are approximately three times greater in Zones 2 and 3 in relation to Zone 1. Nevertheless, the topographic parameter of the distribution of heights in relation to the mid-plane (S_{sk}) shows a homogeneous roughness behavior in Zones 1 and 2 (this is inferred because $S_{sk} \cong 0$). It also shows the presence of peaks or discontinuities in Zone 3 ($S_{sk} > 0$). The value of the kurtosis ($S_{ku} \cong 3$) in Zones 1 and 2 corroborate its homogeneity, while the value in Zone 3 ($S_{ku} > 3$) corroborates the high number of irregularities in this zone.

Discussion

Cutting process kinematics

During the finishing process on the flat surface, the direction of the effective cutting speed vector and the chip morphology are the same for every cross-feed pass. On the other hand, in the finishing process on the concave and convex surfaces, these two variables change in relation to the radii of curvature of the machined surface and in relation to the tilt angle (φ) that varies in each cross-feed pass. Equation (1) shows the parametric formulation of the revolution elliptical toroid (which generates the work surface) $\boldsymbol{r}_{\mathbf{P}}$ in function of the parameters (U_{P}, V_{P}). In it, a and b are semiaxes of the ellipse, and (h, k) is the geometric center of the ellipse on the X–Y plane. The directions of the tangent vectors $\boldsymbol{u}_{\mathbf{P}}$ and $\boldsymbol{v}_{\mathbf{P}}$ agree with the cross-feed and the feed movement of the machining process, respectively. The cross product of these two vectors defines the surface normal vector $\boldsymbol{n}_{\mathbf{P}}$ [Equation (2)], on which

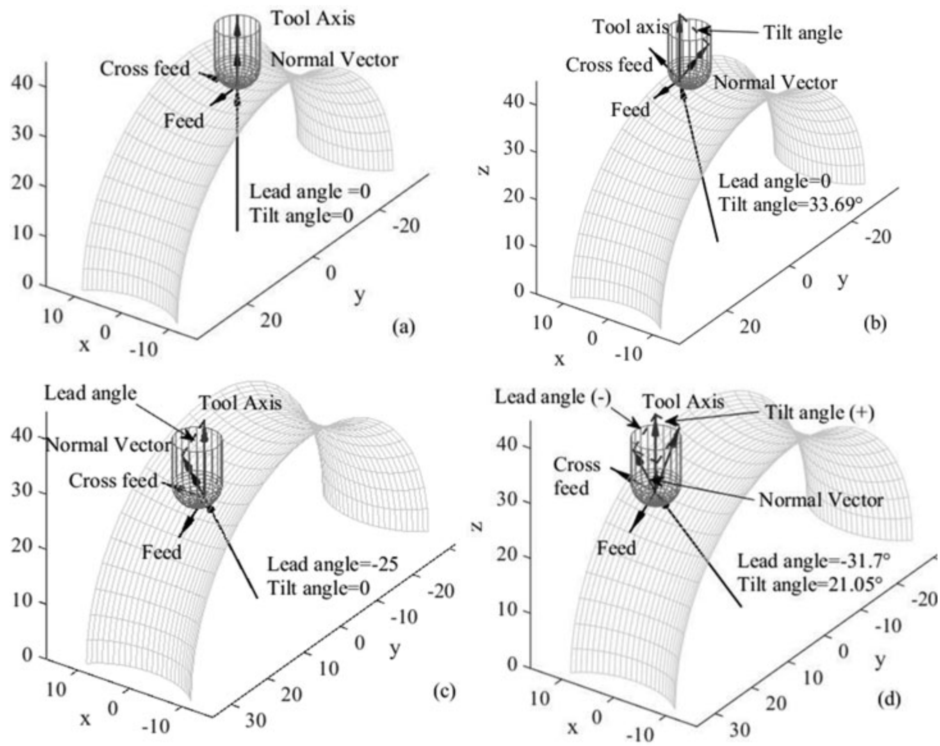

Figure 4. Variation of the lead (β) and tilt (φ.) angles depending on the orientation of the tool axis in reference to the normal vector to the surface.

the center of the ball-end tool is found. Defining a reference system with these three vectors, the inclination angles between the tool axis and surface normal vector can be determined, as shown in Figure 4.

$$\boldsymbol{r}_\mathrm{P} = \boldsymbol{r}_\mathrm{P}\left(U_\mathrm{P}, V_\mathrm{P}\right) = \begin{bmatrix} X_\mathrm{P}(U_\mathrm{P}, V_\mathrm{P}) \\ Y_\mathrm{P}(U_\mathrm{P}, V_\mathrm{P}) \\ Z_\mathrm{P}(U_\mathrm{P}, V_\mathrm{P}) \end{bmatrix} = \begin{bmatrix} h + a\cos\cos U_\mathrm{P} \\ (k + b\sin\sin U_\mathrm{P})\cos\cos V_\mathrm{P} \\ (k + b\sin\sin U_\mathrm{P})\sin\sin V_\mathrm{P} \end{bmatrix} \tag{1}$$

$$\boldsymbol{U}_\mathrm{P} = \frac{\partial r_\mathrm{P}}{\partial U_\mathrm{P}};\ \boldsymbol{V}_\mathrm{P} = \frac{\partial r_\mathrm{P}}{\partial V_\mathrm{P}};\ \boldsymbol{u}_\mathrm{P} = \frac{\mathbf{U_P}}{|\mathbf{U_P}|};\ \mathbf{v_P} = \frac{\mathbf{V_P}}{|\mathbf{V_P}|};\ \mathbf{n_P} = \mathbf{u_P} \times \mathbf{v_P} \tag{2}$$

The inclination angle in the feed direction is called lead angle (β) and it is positive if the tool axis is tilted in the feed direction. The inclination angle in the cross-feed direction is the tilt angle (φ) and it is positive if the tool axis is tilted in the cross-feed direction. Figure 4a shows the tool in a position in which the directions of the tool axis vector and the surface normal vector are aligned. In this case, the lead and tilt inclination angles are zero. Due to the architecture of the machine and the curvature variability of the surface, if the tool moves in the cross-feed direction, a tilt angle is induced (Figure 4b). If the tool moves in the feed direction, a lead angle is induced (Figure 4c). Figure 4d shows the tool in a position on the surface where there are variations in both the lead (β) and tilt (φ) angles. To determine the tilt angle, the tool axis is projected on the plane generated by the cross-feed vector and the surface

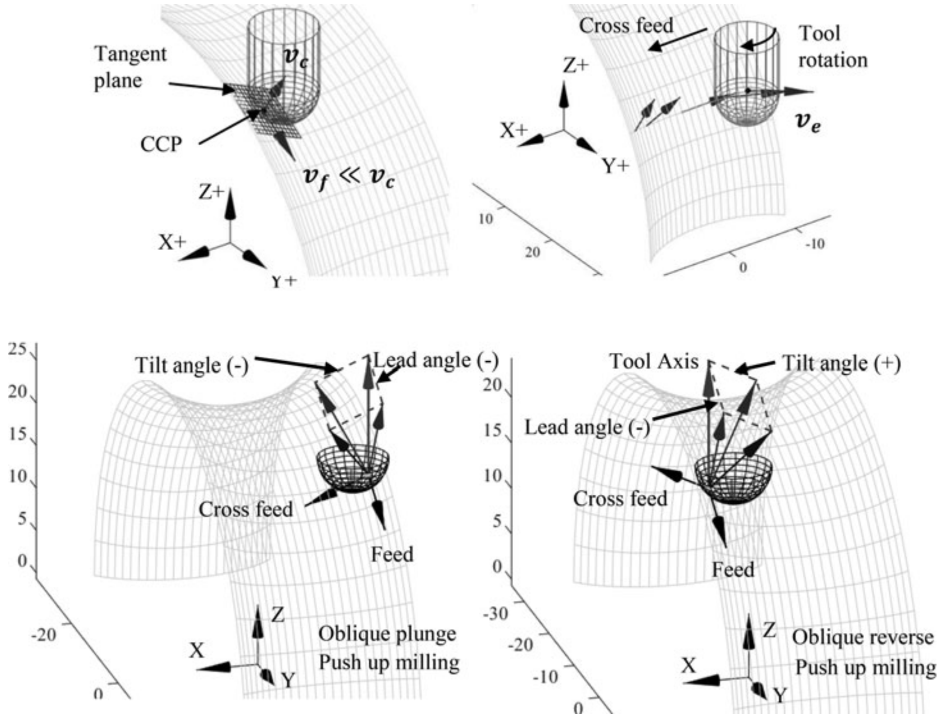

Figure 5. Kinematic analysis of the concave surface machining process.

normal vector. To determine the lead angle, the tool axis is projected on the plane generated by the feed speed vector and the surface normal vector.

The variation of the angle between the tool axis and surface normal vector induced a change in the magnitude and direction of the effective cutting speed vector $\boldsymbol{v}_{\mathbf{e}}$ which defines the direction of the chip formation (Radzevich, 2008). The $\boldsymbol{v}_{\mathbf{e}}$ vector is located on the tangent plane $\boldsymbol{T}_{\mathbf{P}}$ to the surface, represented by Equation (3) (Toponogov, 2006), at the cutter contact point (CCP) between the machined surface and cutting surface of the tool, as illustrated in Figure 5.

$$\boldsymbol{T}_{\mathrm{P}} \Rightarrow \begin{bmatrix} \left(\boldsymbol{r}_{\mathrm{tp}} - \boldsymbol{r}_{\mathrm{p}}^{(\mathrm{CCP})}\right) \\ \boldsymbol{u}_{\mathrm{P}} \\ \boldsymbol{v}_{\mathrm{P}} \end{bmatrix} = 0 \tag{3}$$

The cutting speed $\boldsymbol{v}_{\mathbf{c}}$ and feed speed $\boldsymbol{v}_{\mathbf{f}}$ vectors are also found on the tangent plane and they are defined by Equation (4), where $\boldsymbol{\omega}_{\mathbf{tool}}$ and $\boldsymbol{\omega}_{\mathbf{wp}}$ correspond to the rotational speed of the tool and to the rotational speed of the raw material, respectively. The vector $\boldsymbol{r}_{\mathbf{tool}}$ represents the radius of the tool, and the vector $\boldsymbol{r}_{\mathbf{p}}$ represents the distance from the rotation center of the raw material to the CCP. The effective cutting speed vector $\boldsymbol{v}_{\mathbf{e}}$ of the movement of the tool edge in reference to the surface is determined by the vector sum of the cutting speed vector $\boldsymbol{v}_{\mathbf{c}}$ with the feed speed vector $\boldsymbol{v}_{\mathbf{f}}$, but for this case $\boldsymbol{v}_{\mathrm{c}} \gg \boldsymbol{v}_{\mathrm{f}}$, it is considered that $\boldsymbol{v}_{\mathrm{e}} \cong \boldsymbol{v}_{\mathrm{c}}$. At the top right-hand side of Figure 5, it is seen that the direction of the effective cutting speed vector $\boldsymbol{v}_{e}$ varies as it makes its cross-feed in the direction of the $X+$ axis.

$$\boldsymbol{v}_{\mathrm{c}} = \boldsymbol{\omega}_{\mathbf{tool}} \times \boldsymbol{r}_{\mathbf{tool}};\ \boldsymbol{v}_{\mathrm{f}} = \boldsymbol{\omega}_{\mathrm{wp}} \times \boldsymbol{r}_{\mathrm{P}};\ \boldsymbol{v}_{\mathrm{e}} = \boldsymbol{v}_{\mathrm{c}} + \boldsymbol{v}_{\mathrm{f}} \tag{4}$$

According to the nomenclature proposed by Bouzakis et al. (2003), a push-up milling occurred in the experimental setup with $\beta' = -25°$ on the concave surface. It shows a variation of the lead angle in the feed direction between $\beta = -25°$ and $-30°$ and a variation in the tilt angle between $\varphi = -37°$ and $37°$, which produces a transition from an oblique-plunge-push-up milling to an oblique-reverse-push-up milling as it moves forward in the cross-feed direction (Figure 5). For the experimental setup to the $\beta' = -60°$ angle, the β angle varies between $\beta = -60°$ and $-65°$, and the tilt angle varies between$\varphi = -37°$ and $37°$.

Modeling of chip thickness

Figure 6 shows the experimental setup for the ball-end milling process of the flat surface and the kinematic behavior associated with the discrete 3D geometry of the nondeformed chip. It also shows the variation behavior of the nondeformed chip thickness during the formation process for tilted surfaces to the lead angle $\beta = -25°$ and $-60°$. In both cases, it is observed that the chip formation process proceeds from the greatest to smallest chip thickness (push-up milling) and there were no relevant differences in the quality of the machined surfaces. This explains why there was no smeared/adhered material on the flat surfaces either in the titanium alloy or

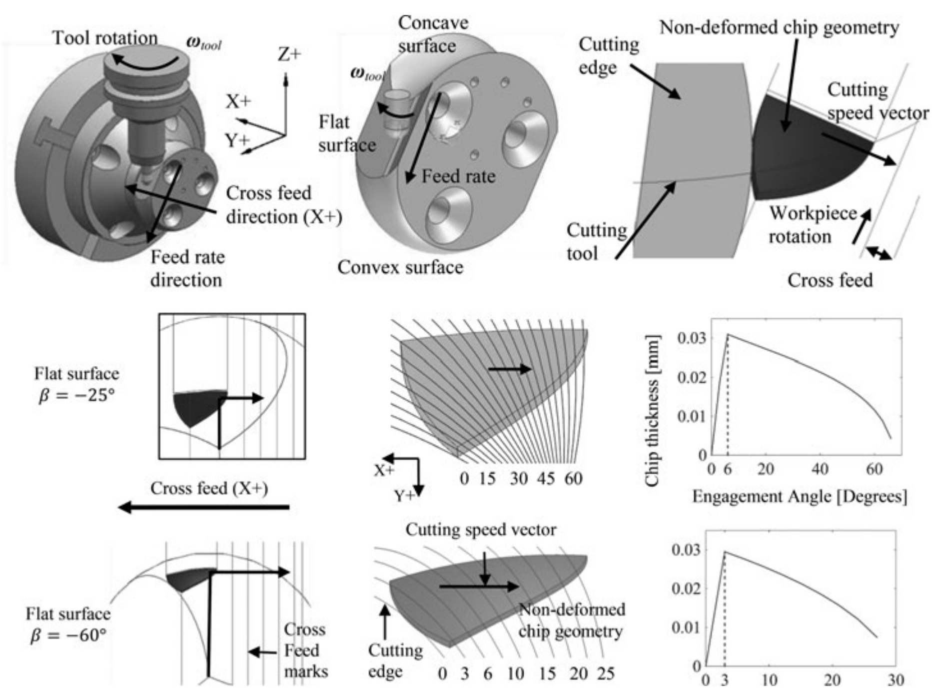

Figure 6. Nondeformed chip and discrete model in the flat surface machining. Thickness variation of the nondeformed chip $\beta = -25°$ and $-60°$.

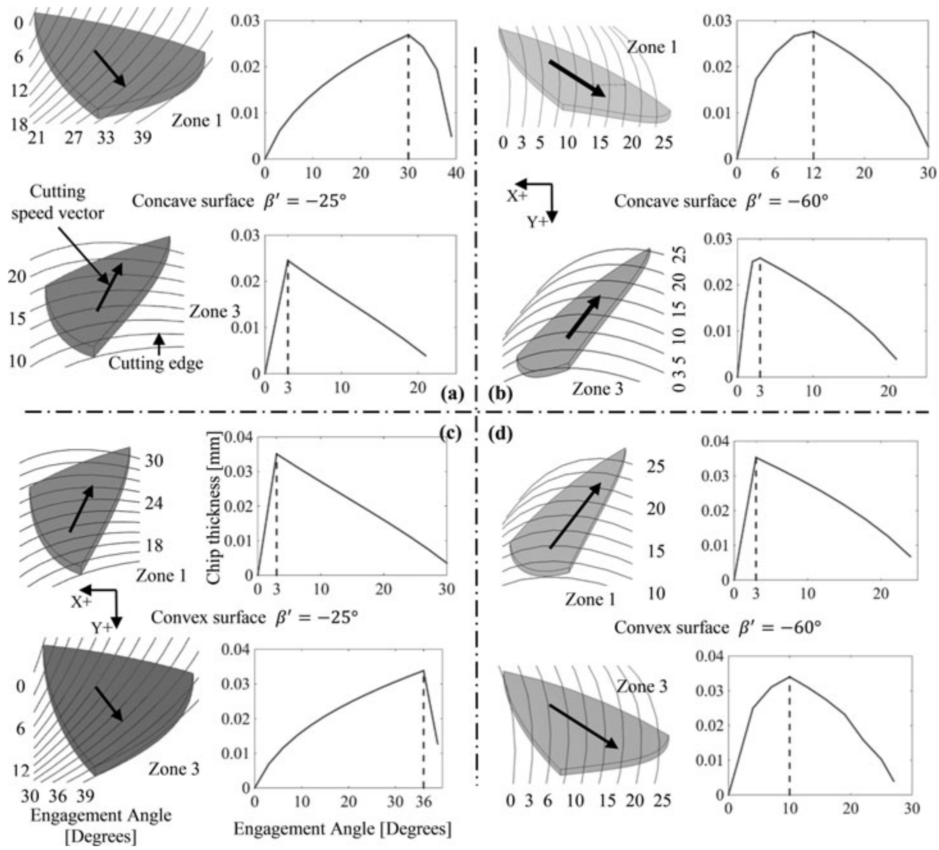

Figure 7. Thickness variation of the nondeformed chip in the concave and convex surfaces.

in the aluminum alloy, as shown in Figure 2. The effective cutting speed is lower for $\beta = -25°$ (29.2 m/min) than for $\beta = -60°$ (59.8 m/min). The engagement angle is closer to 60° for $\beta = -25°$, approximately double than that for $\beta = -60°$.

Figure 7 shows the discrete nondeformed chip 3D models on the concave and convex surfaces for $\beta' = -25°$ and for $\beta' = -60°$. It also illustrates the position angle of the tool edge and the geometric evolution of thickness of the nondeformed chip. Figure 7a shows the top view of the nondeformed chip in the finishing process on the concave machined surface with $\beta' = -25°$ angle. In Zone 1 (negative tilt angle), oblique-plunge-push-up milling is presented and it is observed that the maximum thickness of the chip is seen when almost finishing the contact. The cut is therefore characterized by high friction and by difficulty in the initial formation of the chip. A smeared/adhered material was observed on the surface in this zone in the titanium alloy but not in the aluminum alloy.

The material adhered on the machined surfaces of the titanium alloy when the tilt angle is negative can be explained by the interaction of three phenomena. First, there is a fact of the kinematic geometry that produces an initial nondeformed chip thickness with almost zero value. Second, the titanium's work-hardening characteristics are such that during machining a high shearing angle is formed. This causes a thin chip to contact a relatively small area on the cutting tool face and results in high bearing loads per unit area. The high bearing force, combined with the friction developed by the chip as it rushes over the bearing area, results in a great increase in heat (Donachie, 2000). Third, in the machining titanium alloys, the occurrence of thermoplastic instability (also called adiabatic shear) within the primary shear zone is generally accepted, which occurs when the rate of thermal softening exceeds the rate of strain hardening (Barry et al., 2001).

Unlike the titanium alloy, in the case of the aluminum alloy, no material adhered under any condition of the ball-end milling process was observed. This is mainly attributed to the higher machinability of aluminum alloy as compared with that of the titanium alloy. The titanium alloy has twice the hardness, a 60% higher ultimate tensile strength, a higher percentage of elastic elongation, and thermal conductivity 20 times lower than that of the aluminum alloy (Table 1). Moreover, zinc, cooper, and magnesium as alloying elements of the aluminum alloy, facilitate the chip formation process during the machining of this material. There was no adhered material on the machined surface in Zone 3 (positive tilt angle), where oblique-reverse-push-up milling was presented either in the titanium alloy or in the aluminum alloy, where greatest chip thickness occurred almost at the initial contact.

Figure 7b shows the top view of the nondeformed chip on the machined concave surface with a $\beta' = -60°$ angle (greater cutting speed). In Zone 1 (oblique-plunge-push-up milling), it is seen that the highest chip thickness was reached in an intermediate position of the engagement angle that the one shown in Zone 1 for the machined surface with $\beta' = -25°$ angle. It is remarkable that a lesser quantity of adhered chips was observed on this surface in the titanium alloy. An oblique-reverse-push-up milling cut was seen mainly in Zone 3 (positive tilt angle), but no chips were observed adhered to the machined surfaces in either of the alloys.

Figure 7c shows the top view of the nondeformed chip on the convex machined surface with a $\beta' = -25°$ angle. In Zone 1 (positive tilt angle—oblique-reverse-push-up milling), no chips were found adhered to the surfaces (Figures 2 and 3). Zone 3 (negative tilt angle—oblique-plunge-push-up milling) shows the beginning of the chip formation from the least to the greatest thickness that explains partially both the large amount of chip fragments that adhered to the machined surface and high roughness value in the titanium alloy (Figures 2 and 3).

Figure 7d shows the top view of the chip formation process on the convex machined surface with a $\beta' = -60°$ angle (greater cutting speed). No chips adhered to the surface in Zone 1 (positive tilt angle—oblique-reverse-push-up milling). Chips were found adhered to the surface in Zone 3 (negative tilt angle—oblique-plunge-push-up milling) in the titanium alloy, but with a lower intensity than where the machining was done with a $\beta' = -25°$ angle. The lesser occurrence of defects can be attributed partially to the chip formation process, which is minimum at the beginning and reaches the maximum height at an intermediate contact angle (10°). Compared with Figure 7c, it can be observed that for $\beta' = -25°$, the maximum chip height is reached at the end of the contact.

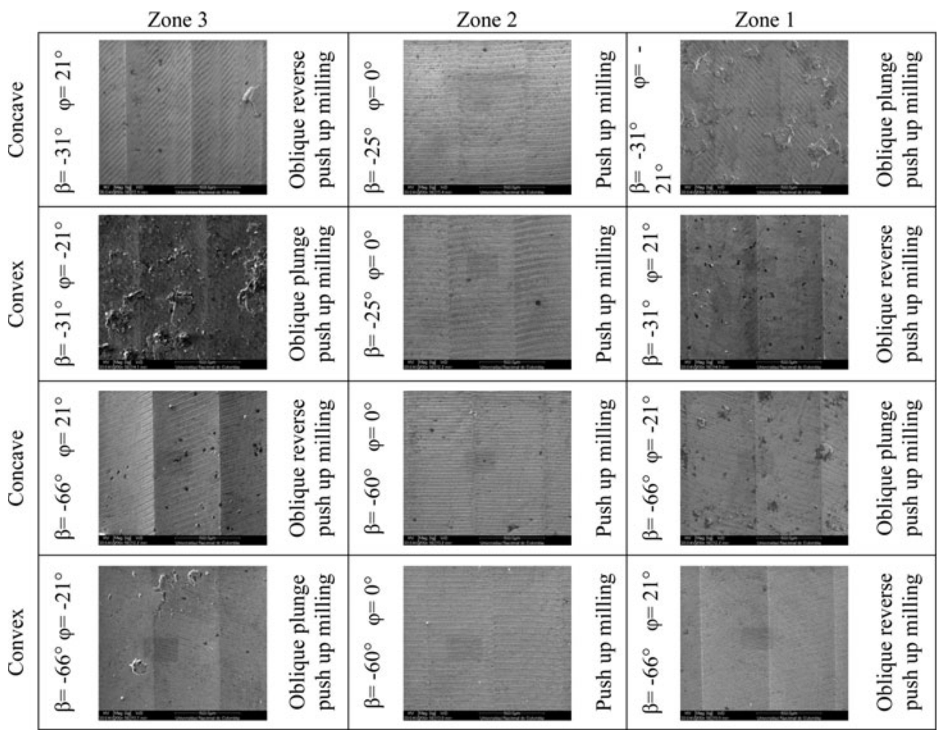

Figure 8. Scanning electron microscope images of different zones of *Ti-6Al-4V* alloy (200×).

Figure 8 summarizes the appearance of the defect smeared/adhered material depending on the angles of inclination of the tool in different zones of the concave and convex surfaces.

Conclusion

In the machining of freeform surfaces, kinematics of the process and the surface curvature directly influence the angle between the tool axis and surface normal vector. This induces changes in the lead and tilt angles, so it modifies the chip geometry, chip formation process, and magnitude and direction of the cutting speed vector.

The flat surfaces were machined using the push-up milling strategy with a $\varphi = 0°$ tilt angle and $\beta = -25°$ and $-60°$ lead angles. The chip formation modeling showed maximum thickness of the chip when beginning the contact and the surfaces obtained did not show defects. The concave and convex surfaces were also machined using the push-up milling strategy with $\beta' = -25°$ and $-60°$ lead angles. The surface geometry caused a variation in the tilt angle between $\varphi = -37°$ and $37°$ for the convex surfaces and between $\varphi = 37°$ and $-37°$ for the concave surfaces.

The modeling of the chip formation shows that the machining process presents a gradual variation from the oblique-plunge-push-up milling to the oblique-reverse-push-up milling for each new cross-feed pass, on the concave surface as well as on the convex surface. In the oblique-plunge-push-up milling on the concave surface, when the tilt angle is negative, mainly smeared/adhered material was seen mainly in the *Ti-6Al-4V* alloy. In the aluminum alloy, no defects due to oblique-plunge-push-up milling were observed.

The intensity of the defects, in the titanium alloy increases with the negative increment of the tilt angle (oblique-plunge-push-up milling). With the positive tilt angles, no defects were observed on the surfaces. The surfaces with the best quality were obtained with the greatest positive tilt angles (oblique-reverse-push-up milling). The increment of lead angle in a negative direction ($\beta = -60°$) decreased the presence of smeared/adhered material on the machined curved surfaces in the titanium alloy. Despite the fact that the cutting speed increases with a greater negative lead angle, the least occurrence of defects happened when the maximum chip thickness tends to occur at the beginning of the chip formation.

It was observed that smeared/adhered material does not appear in 7075 aluminum alloy during the oblique-plunge-push-up milling; this is explained because this aluminum alloy has greater machinability than that of the *Ti-6Al-4V* titanium alloy. On the other hand, the smeared/adhered material on the machined surfaces of titanium alloy can be explained by the interaction of several factors: the high friction and difficulty of the initial formation of the chip in oblique-plunge-push-up milling; the high tensile strength of this titanium alloy along with its low elastic modulus; and its work-hardening characteristics plus its thermoplastic instability during machining processing.

The geometric modeling of the evolution of thickness of nondeformed chips made it possible to conclude that in the finishing milling process with a ball-end tool on surfaces with radii of curvature different from zero, maximum chip thickness occurred in intermediate positions that do not correspond to either the beginning or the end of the chip formation process.

Acknowledgments

The authors acknowledge the funding received from Colciencias (Contract RC723-2011) and from the Research Division of the Universidad Nacional de Colombia (DIB2030100). The physical assembly was implemented in the Laboratorio Fabrica Experimental (LabFabEx). The digital setup was done in the Laboratorio de Manufactura Multieje of Universidad Santo Tomás.

Nomenclature

- a Semiaxis of the ellipse, mm
- b Semiaxis of the ellipse, mm
- β Lead angle, °
- β' Angle between the tool axis and the surface normal vector projection on the Y–Z plane, °
- CCP Cutter contact point
- h Geometric center of the ellipse (X coordinate), mm
- k Geometric center of the ellipse (Y coordinate), mm

$\boldsymbol{n}_{\mathbf{P}}$	Unit normal vector to the surface P at CCP
P	Surface
$\boldsymbol{r}_{\mathbf{P}}$	Position vector of a point of the surface P, mm
$\boldsymbol{r}_{\mathbf{tool}}$	Position vector of the surface of the tool at CCP, mm
$\boldsymbol{r}_{\mathbf{tP}}$	Position vector of a point of the tangent plane to the surface P at CCP, mm
$\boldsymbol{r}_{\mathbf{P}}^{\mathbf{CCP}}$	Position vector of the point CCP on the surface P, mm
S_{a}	Surface roughness, μm
S_{q}	Root mean squared roughness, μm
S_{sk}	Skewness
S_{ku}	Kurtosis
$\boldsymbol{T}_{\mathbf{P}}$	Tangent plane
$\boldsymbol{u}_{\mathbf{P}}$	Unit tangent vector of the surface with respect to parameter U_{P}
$\boldsymbol{U}_{\mathbf{P}}$	Tangent vector of the surface with respect to parameter U_{P}
U_{P}	Parameter of the surface equation
$\boldsymbol{v}_{\mathbf{c}}$	Cutting speed vector, m/min
$\boldsymbol{v}_{\mathbf{e}}$	Effective cutting speed vector, m/min
$\boldsymbol{v}_{\mathbf{f}}$	Feed speed vector, m/min
$\boldsymbol{v}_{\mathbf{P}}$	Unit tangent vector of the surface with respect to parameter U_{P}
$\boldsymbol{v}_{\mathbf{P}}$	Tangent vector of the surface with respect to parameter, V_{P}
V_{P}	Parameter of the surface equation
$\omega_{\mathbf{tool}}$	Rotational speed of the tool, rad/s
$\omega_{\mathbf{wp}}$	Rotational speed of the workpiece, rad/s
X	Cartesian coordinate, mm
Y	Cartesian coordinate, mm
φ	Tilt angle, °
Z	Cartesian coordinate, mm

ORCID

Jorge Andrés García-Barbosa http://orcid.org/0000-0002-7020-4688
José Manuel Arroyo-Osorio http://orcid.org/0000-0003-3636-8029
Ernesto Córdoba-Nieto http://orcid.org/0000-0002-6527-1069

References

Barry, J.; Byrne, G.; Lennon, D. (2001) Observations on chip formation and acoustic emission in machining Ti-6Al-4V alloy. *International Journal of Machine Tools and Manufacture*, *41*: 1055–1070.

Becze, C.E.; Clayton, P.; Chen, L.; El-wardany, T.I.; Elbestawi, M.A. (2000) High-speed five-axis milling of hardened tool steel. *International Journal of Machine Tools and Manufacture*, *40*: 869–885.

Bouzakis, K.; Aichouh, P.; Efstathiou, K. (2003) Determination of the chip geometry, cutting force and roughness in free form surfaces finishing milling, with ball end tools. *International Journal of Machine Tools and Manufacture*, *43*: 499–514.

Cheharon, C.; Jawaid, A. (2005) The effect of machining on surface integrity of titanium alloy Ti–6% Al–4% V. *Journal of Materials Processing Technology*, *166*: 188–192.

Donachie, M.J. (2000) *Titanium: A Technical Guide*. ASM International, OH, USA.

Ezugwu, E.O.; Wang, Z.M. (1997) Materials titanium alloys and their machinability—A review. *Journal of Materials Processing Technology*, *68*: 262–274.

Fagali de Souza, A.; Diniz, A.E.; Rodrigues, A.R.; Coelho, R.T. (2014) Investigating the cutting phenomena in free-form milling using a ball-end cutting tool for die and mold manufacturing. *International Journal of Advanced Manufacturing Technology*, *71*: 1565–1577.

García-Barbosa, J.A.; Arroyo-Osorio, J.M.; Córdoba-Nieto, E. (2014) Simulation and verification of parametric numerical control programs using a virtual machine tool. *Production Engineering*, *8*: 1–7.

Ginting, A.; Nouari, M. (2009) Surface integrity of dry machined titanium alloys. *International Journal of Machine Tools and Manufacturing*, *49*: 325–332.

Guo, Y.B.; Li, W.; Jawahir, I.S. (2009) Surface integrity characterization and prediction in machining of hardened and difficult-to-machine alloys: A state-of-art research review and analysis. *Machining Science and Technology: An International Journal*, *13*: 437–470.

Hood, R.; Johnson, C.M.; Soo, S.L.; Aspinwall, D.K.; Sage, C. (2014) High-speed ball nose end milling of burn-resistant titanium (BuRTi) alloy. *International Journal of Computer Integrated Manufacturing*, *27*: 139–147.

Li, A.; Zhao, J.; Luo, H.; Zheng, W. (2011) Machined surface analysis in high-speed dry milling of Ti-6Al-4V alloy with coated carbide inserts. *Advanced Materials Research*, *325*: 412–417.

Lin, R.S.; Koren, Y. (1996) Efficient tool-path planning for machining free-form surfaces. *Journal of Engineering for Industry*, *118*(1): 20–28.

Mhamdi, M.; Boujelbene, M.; Bayraktar, E.; Zghal, A. (2012) Surface integrity of titanium alloy Ti-6Al-4V in ball end milling. *Physics Procedia*, *25*: 355–362.

Quinsat, Y.; Lavernhe, S.; Lartigue, C. (2011) Characterization of 3D surface topography in 5-axis milling. *Wear*, *271*(3–4): 590–595.

Radzevich, S. (2008) *Kinematic Geometry of Surface Machining*. CRC Press, Taylor & Francis Group, Boca Raton, FL, USA.

Sun, J.; Guo, Y.B. (2009) A comprehensive experimental study on surface integrity by end milling Ti-6Al-4V. *Journal of Materials Processing Technology*, *209*: 4036–4042.

Thomas, M.; Turner, S.; Jackson, M. (2010) Microstructural damage during high-speed milling of titanium alloys. *Scripta Materialia*, *62*: 250–253.

Toponogov, V.A. (2006) *Differential Geometry of Curves and Surfaces*. Birkhäuser, Boston, MA.